

Article

Polymer-Modified Cellulose Nanofibrils Cross-Linked with Cobalt Iron Oxide Nanoparticles as a Gel Ink for 3D Printing Objects with Magnetic and Electrochemical Properties

Jakob Benedikt Mietner ¹, Sebastian Willruth ², Rajesh Kombar ³, Christoph Gimmler ³, Bilal Nehmeh ⁴ and Julien R. G. Navarro ^{1,*}

¹ Institute of Wood Science, University of Hamburg, Haidkrugsweg 1, 22885 Barsbüttel-Willinghusen, Germany

² Department of Chemistry, University of Hamburg, Grindelallee 117, 20146 Hamburg, Germany

³ Fraunhofer Center for Applied Nanotechnology CAN–(Research Division of Fraunhofer IAP), Grindelallee 117, 20146 Hamburg, Germany

⁴ Department of Natural Sciences, School of Arts and Sciences, Lebanese American University, Beirut 1102 2801, Lebanon

* Correspondence: julien.navarro@uni-hamburg.de; Tel.: +49-40-7396-2612

Abstract: This paper presents a strategy to convert hydrophilic cellulose nanofibrils (CNF) into a highly cross-linked hydrophobic network with inorganic nanoparticles to develop a gel ink suitable for gel 3D printing. The CNF were chemically modified initially through a single-electron transfer-living radical polymerization (SET-LRP) of stearyl acrylate (SA) in the presence of the surface-modified cobalt iron oxide (CoFe₂O₄, CFO) nanoparticles. The modified CFO nanoparticles provide their multifunctional properties, such as magnetic and electrochemical, to the CNF hybrid network and, at the same time, act as cross-linking agents between the nanocellulose fibrils, while the grafted poly-stearyl acrylate (PSA) introduces a strong hydrophobicity in the network. A suitable gel ink form of this CNF–PSA–CFO material for gel 3D printing was achieved together with a certain solvent. Some test structure prints were directly obtained with the CNF–PSA–CFO gel and were used to evaluate the consolidation of such 3D objects through solvent exchange and freeze-drying while also keeping the magnetic and electrochemical properties of CFO in the CNF-based composite intact. The pristine CNF and CFO particles and the CNF–PSA–CFO were characterized by FTIR, SEM, XPS, TGA, VSM, and CV measurements.

Keywords: cellulose nanofibrils; single-electron transfer-living radical polymerization (SET-LRP); grafting-from; nanoparticles; cross-linking; CoFe₂O₄; gel 3D printing; electrochemical–magnetic properties



Citation: Mietner, J.B.; Willruth, S.; Kombar, R.; Gimmler, C.; Nehmeh, B.; Navarro, J.R.G. Polymer-Modified Cellulose Nanofibrils Cross-Linked with Cobalt Iron Oxide Nanoparticles as a Gel Ink for 3D Printing Objects with Magnetic and Electrochemical Properties. *Fibers* **2023**, *11*, 2. <https://doi.org/10.3390/fib11010002>

Academic Editors: Jungmok You and Jeonghun Kim

Received: 15 November 2022

Revised: 13 December 2022

Accepted: 19 December 2022

Published: 21 December 2022



Copyright: © 2022 by the authors. Licensee MDPI, Basel, Switzerland. This article is an open access article distributed under the terms and conditions of the Creative Commons Attribution (CC BY) license (<https://creativecommons.org/licenses/by/4.0/>).

1. Introduction

One of the greatest challenges for a future sustainable society is the use of renewable and environmentally friendly material resources that can replace fossil-based products to produce high-performance functional materials. Therefore, in recent decades more and more attention has been given to the utilization of bio-based polymers such as cellulose, which offers many advantages, for instance, being renewable, biodegradable, and recyclable [1–6]. Some of the most interesting cellulose-based materials are cellulose nanofibrils (CNFs) which exhibit numerous intrinsic advantages, including high elastic modulus, remarkable strength, high specific surface area, and high aspect ratio, which make them promising for a variety of applications ranging from drug delivery and water purification to composites [7–10].

One step further is to combine cellulose nanofibrils and inorganic nanoparticles to create hybrid bio-based materials. Such materials have attracted much interest since they combine organic and inorganic components and allow the individual properties of

each component to be incorporated into the final material. Various research groups have developed said hybrid materials made of nanocellulose and inorganic nanoparticles. Guo et al. [11] included gold nanoparticles into CNF by azide-alkyne-Huisgen cycloaddition or by electrostatic interactions between a positively charged CNF and the negatively charged nanoparticles. This CNF-based hybrid material with gold nanoparticles can then be used as a substrate for surface-enhanced Raman scattering [12]. Dadigala et al. [13] prepared material from CNF-supported Pd nanoparticles as a novel nanozyme with good peroxidase and oxidase-mimicking activities and easy recyclability for the remediation of water pollution, which was shown by dye degradation in a continuous flow method. Other research groups immobilized quantum dot nanoparticles onto nanocellulose [14–17] and showed potential applications in bio-labeling, photoelectrical ink, and integrated optical electronic and light-emitting devices. Another example is the combination of vanadium oxide and nanocellulose to produce a stimuli-responsive chromium paper device [18–21]. In the above cases, nanocellulose and inorganic nanoparticles were connected either by covalent bonding/coupling or electrostatic interaction.

In our recent publications [22–25], we have shown that hydroxide groups on the CNF surface can be chemically modified to act as a radical polymerization initiator. Single-electron transfer-living radical polymerization (SET-LRP), introduced by Percec et al. [26–31], is a form of Cu(0)-mediated radical polymerization and has been used as a powerful polymerization technique since the reaction is normally not influenced by the presence of water and noninert conditions [32–36]. This kind of Cu(0)-mediated free radical polymerization can be used to polymerize either hydrophilic or hydrophobic vinyl monomers, with the additional advantage that the length of the polymer chain can be fully controlled [37–40].

We also demonstrated an approach of cross-linking polymer-modified cellulose nanofibrils with inorganic nanoparticles through surface-initiated grafting from SET-LRP [24]. The controlled radical polymerization of stearyl acrylate in the presence of modified barium titanate nanoparticles has improved the properties of the CNF drastically by restricting the interfibril interaction upon drying, while the barium titanate nanoparticles add their properties to the final hybrid material.

Recently, it has been shown that CNF-containing materials are promising candidates to be used in the 3D printing processes [41–48]. Three-dimensional printing, also referred to as rapid prototyping, is a fairly new processing technology that allows the production of customized objects through a layer-by-layer process. Such 3D-printed CNF-based objects have enormous potential as, for example, printed bioactive composites used in tissue engineering, wound dressings, and printed tablets for the controlled release of drugs [20,49,50]. However, the 3D printing of such CNF gel should exhibit a shape fidelity and stability of the desired object after the printing. For this reason, and to increase the mechanical properties of the gel, a cross-linking process of the CNF is necessary.

Markstedt et al. [51] created a bio-ink made of cross-linked CNF, alginate, and CaCl_2 . The cross-linked CNF–alginate material proved to be a feasible support for hosting human nasoseptal chondrocyte cells. Leppiniemi et al. [52] developed a CNF-based gel ink with alginate, the protein avidin, and glycerin. In this study, Leppiniemi et al. used CaCl_2 as a cross-linker and CNF as a strengthening additive, which led to better shape fidelity after 3D printing. Moreover, the 3D-printed object showed high tissue compatibility and great potential in biomedical wound dressings applications. Li et al. [53] used nanocellulose and carbon nanotubes for 3D printing. A possibility to 3D print CNF-based gels made of oxidized CNF, cross-linked with various metal cations, was demonstrated by our group previously [54].

CFO nanoparticles show very high potential in several electrochemical applications [55], such as supercapacitors [56,57], electrochemical sensing [58], and as anode materials for sodium ion [59] or lithium-ion [60] batteries. CFO nanoparticles are as well known for their magnetic characteristics. Interestingly, the magnetic properties, either paramagnetic [61,62] or superparamagnetic [63], can be tuned depending on their size. Further, CFO particles

were, for example, used in nanocomposites based on carrageenan, processed by direct ink writing with the ability to be used as magnetic actuators [62].

In this paper, our aim was to develop a bio-based hybrid material made of polymer-modified CNF, cross-linked with CFO nanoparticles, to use as a gel ink for 3D printing. Therefore, CNF was polymer-modified through SET-LRP of stearyl acrylate (SA) in the presence of the surface-modified CFO nanoparticles. The CFO nanoparticles act as a cross-linking agent and impart their electrochemical–magnetic properties to the CNF–PSA–CFO hybrid. By manipulating the solvents, 3D printing gel ink from the CNF–PSA–CFO hybrid was developed and demonstrated.

2. Materials and Methods

2.1. Materials

1,1'-Carbonyldiimidazole (CDI), 2-bromo-2-methylpropionic acid 98%, imidazole $\geq 99\%$, stearyl acrylate (SA, contains 200 ppm monomethyl ether hydroquinone, MEHQ, as inhibitor) 97%, ethyl 2-bromo-2-methylpropionate, 2-acrylamido-2-methyl-1-propanesulfonic acid (AMP) 99%, isopropanol, ethanol 98%, and toluene were purchased from Sigma-Aldrich. Dimethyl sulfoxide (DMSO, $\geq 99\%$) was purchased from Merck/Sigma Aldrich. Tris [2-(dimethylamino)ethyl]amine (Me₆-TREN) was purchased from Alfa Aesar. Copper wire (diameter 1 mm) was purchased from Fisher. Cobalt iron oxide nanoparticles (CoFe₂O₄ nanopowder/nanoparticles, size: 30 nm) were purchased from Nanografi Nano Technology. The dry cellulose source, elemental chlorine-free (ECF) bleached softwood kraft pulp, was obtained from MERCER Stendal GmbH, Germany. The Northern bleached softwood Kraft pulp was made from pine (30–60%) and spruce (40–70%). CNF was produced by processing the softwood Kraft pulp with an M-110EH-30 Microfluidizer from Microfluidics.

2.2. Extraction of Cellulose Nanofibrils from Wood Pulp

The CNF was prepared according to a previously reported procedure [54]. Briefly, the cellulose pulp was firstly suspended in water and then ground to obtain a 75–80° SR (SR: Schopper-Riegler degrees, determined using the Schopper–Reigler method (DIN EN ISO 5267-1)). After that, the ground slurry was further refined with a microfluidizer under high pressure by passing the slurry several times in different chambers with orifice widths of 400 μm and 200 μm (2 times, 15,000 psi) and 200 μm and 100 μm (4 times, 25,000 psi) successively. The process resulted in a 2.1 wt% CNF aqueous gel.

2.3. Prepolymerisation Modification of the CNF

The water-based CNF gel was solvent exchanged with DMSO according to a previously published method [24]. Briefly, DMSO was slowly added to the CNF suspension under constant stirring. The CNF suspension was then centrifuged (4000 rpm/20 min), and the supernatant (DMSO and water) was discarded and replaced with fresh DMSO. The procedure was repeated 4 times. After that, a CNF-based macroinitiator (CNF-MI) was obtained by grafting an initiator unit on the CNF with 2-bromo-2-methylpropionic acid in the same way as in one of our previous papers [24]. The process resulted in a 1.0 wt% gel of CNF-MI in DMSO.

2.4. Surface Modification of CFO Nanoparticles

A total of 50 mg of CFO nanoparticle powder was suspended in 100 mL of ethanol. Then, 2-Acrylamido-2-methyl-1-propanesulfonic acid (1.0 g, 4.8 mmol) in 10 mL of ethanol was added to the nanoparticles suspension, and the suspension was then stirred and heated to 80 °C for 16 h. The nanoparticles suspension was cooled to room temperature and separated from the liquid phase through centrifugation (6000 rpm, 20 min). The supernatant was removed and replaced with ethanol. After resuspension and centrifugation, the supernatant was replaced with an ethanol/DMSO 1:1 mixture, resuspended, and centrifuged. This operation was repeated 2 times. After that, the modified CFO nanoparticles (CFO-AMP) were suspended in 50 mL of pure DMSO.

2.5. Procedure for SET-LRP Grafting of CNF Together with CFO Nanoparticles (CNF-PSA-CFO)

The SET-LRP reaction procedure is the same as that previously published with barium titanate NPs [24]. A copper wire (1 mm diameter and 6 cm length) was wrapped to a spring shape and immersed in a concentrated hydrochloric acid for 1 min, then rinsed with water and acetone and dried prior to use. The CNF-based macroinitiator (4 g, 1.0 wt%) and the surface-modified CFO nanoparticles (5 mg) were suspended in DMSO (30 mL). SA was dissolved in 15 mL toluene and filtered through a small portion of an aluminum oxide powder to remove the MEHQ polymerization inhibitor. The HCl-treated copper wire was added, and the reaction mixture was degassed via nitrogen purging for 10 min. The temperature was then raised to 40 °C. The polymerization was then started by adding 200 µL Me₆TREN ligand solution (2 vol.% in DMSO), and the reaction was allowed to proceed under a nitrogen atmosphere for 16 h. After cooling to room temperature, the product (CNF-PSA-CFO) was precipitated with isopropanol, and the liquid phase was discarded. CNF-PSA-CFO was washed three times with a toluene/isopropanol (1:4) mixture and collected via centrifugation (4000 rpm/20 min). In the last purification step, CNF-PSA-CFO was dissolved in pure toluene and centrifuged at 50,000 × g for 1.5 h, which resulted in a toluene-based CNF-PSA-CFO gel with a solid content of about 10 wt%.

2.6. Gel 3D Printing

A cube model of 10 × 10 × 5 mm was designed and 3D printed by pneumatic extrusion. Three-dimensional printing was performed with an INKREDIBLE 3D printer from CELLINK. The cubes were 3D printed from a toluene-based gel using a 0.41 mm diameter stainless steel nozzle and a pressure of 30–50 kPa for pneumatic extrusion. For consolidation and drying of the 3D objects, they were first solvent-exchanged from toluene to DMSO in a two-step process. First, the objects were transferred carefully to a 25:75 mixture of DMSO and toluene and stirred slowly overnight. After that, the now-mechanical, more stable objects were transferred to a pure DMSO bath and stirred for another few hours. Then, the objects were frozen in liquid nitrogen and freeze-dried overnight.

2.7. Characterization

Attenuated total reflection Fourier transform infrared spectroscopy (ATR-FTIR) was performed using a Bruker Vector 33 spectrometer. Measurements were performed by accumulating 256 scans in the spectral region of 4000–550 cm⁻¹ with a spectral resolution of 2 cm⁻¹.

The morphology of the different hybrid materials was observed via ultrahigh-resolution field emission scanning electron microscopy (FE-SEM) using a Hitachi S-4800 or SEM LEO (Zeiss) 1550. The dried samples were mounted on sample supports using carbon tape and coated with a 5 nm layer of Pd/Pt with a Cressington 208HR under an inert atmosphere. Some of the pictures were taken with an energy-selective backscattered detector (EsB detector) for enhanced material contrast between organic content and inorganic particles.

XPS Characterization was performed by MSE Analytical Services using Thermo Scientific ESCALAB 250Xi with a source gun type Al K Alpha and a spot size of 400 µm.

Thermal degradation was analyzed with a NETZSCH TG 209 F1 from 25 °C to 600 °C with a 20 K/min ramp under an inert nitrogen atmosphere.

The magnetic moment measurements were performed with an EZ9 from MicroSense. The particles were filled into a ULTEM (Polyetherimide) cup. The cup was glued with double-sided tape to a quartz glass sample holder. Then the sample vibrated at 75 Hz. The field was changed from −25,000 Oe (−2.5 T) to 25,000 Oe (2.5 T) and then back to −25,000 Oe (−2.5 T). The step size was −25,000 to −5000 in 1000 Oe (0.1 T) steps, from −5000 to −1000 Oe in 100 Oe (10 mT) steps, and from −1000 to 1000 Oe in 10 Oe (1 mT) steps.

All electrochemical measurements were performed using an Autolab PGSTAT101 potentiostat. Three-electrode electrochemical measurements were conducted in dry THF, and tetrabutyl ammonium hexafluorophosphate 1 M was used as a supporting electrolyte. A Pt disk was used as working, and a Pt wire was used as counter electrodes. For the

reference electrode, a silver wire was used. The electrolyte solution was purged with argon for 2 min prior to every electrochemical measurement. The reference potential of the silver electrode was calibrated in a solution of $1 \cdot 10^{-3}$ M of Ferrocene in THF.

3. Results and Discussion

A schematic representation for developing the CNF–PSA–CFO material network is shown in Figure 1. Surface-modified CFO (CFO–AMP) particles were combined with the CNF macroinitiator (CNF–MI) in presence of SA monomer to conduct a SET-LRP reaction to realize the multifunctional CNF–PSA–CFO network. Modified CFO act not only as a crosslinking agent but also gives bi-functional—magnetic and electrochemical—properties to the CNF–PSA–CFO network. On the other hand, poly-stearyl acrylate (PSA) introduces a strong hydrophobicity to the network, which helps to develop gel ink for gel 3D printing.

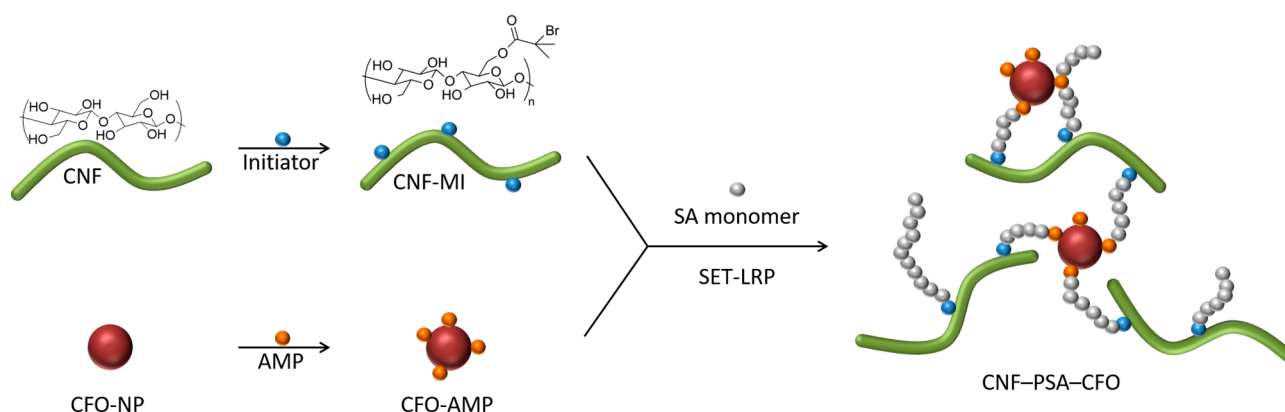


Figure 1. Schematic modification strategy of CNF with PSA and CFO nanoparticles.

The mechanical disintegration of wood pulp with a high-pressure microfluidizer resulted in a 2.1 wt% CNF aqueous gel. On the surface of the CNF, an excessive number of hydroxyl groups are present, which are perfect anchoring centers for potential chemical modifications. To carry out such modification, the water-based CNF gel was first solvent-exchanged with DMSO, and then a CNF-based macroinitiator (CNF-MI) was synthesized by grafting an initiator group unit onto the CNF surface through an esterification reaction with 2-bromo-2-methylpropionic acid [24].

To use CFO nanoparticles as crosslinking agents, they also need to be surface-modified. To let them react directly in the polymerization reaction, they have to be modified with an acrylic function. For that reason, the CFO nanoparticles were surface-modified with 2-Acrylamido-2-methyl-1-propanesulfonic acid by hetero-condensation with the CFO surface hydroxyl groups following a slightly modified previously published method [24,64]. This surface modification also extremely increased the stability of the nanoparticle (NP) suspension in DMSO if compared with the unmodified, crude CFO particles. XPS measurements were performed with the untreated and surface-modified CFO nanoparticles to investigate the elemental composition of the samples and to verify whether the surface modification was successful.

Figure 2a shows the full XPS survey of CFO-AMP. It reveals that the sample consists of cobalt (Co), iron Fe, and oxygen O as well as sulfur S. The high-resolution XPS spectra of Fe2p, Co2p, and O1s are shown in Figure 2 b–d, respectively. In the deconvoluted Fe2p spectrum (Figure 2b), six signals were observed at 710.1, 711.7, 718.1, 723.7, 725.8, and 731.9 eV with the complex multiplet splitting of iron oxides [65,66]. The Co2p high-resolution XPS spectra can be deconvoluted into two peaks at 782.0 eV and 786.7 eV. The O1s peaks at 529.7 and 530.7 eV were assigned to lattice oxygen and surface-adsorbed oxygen, respectively.

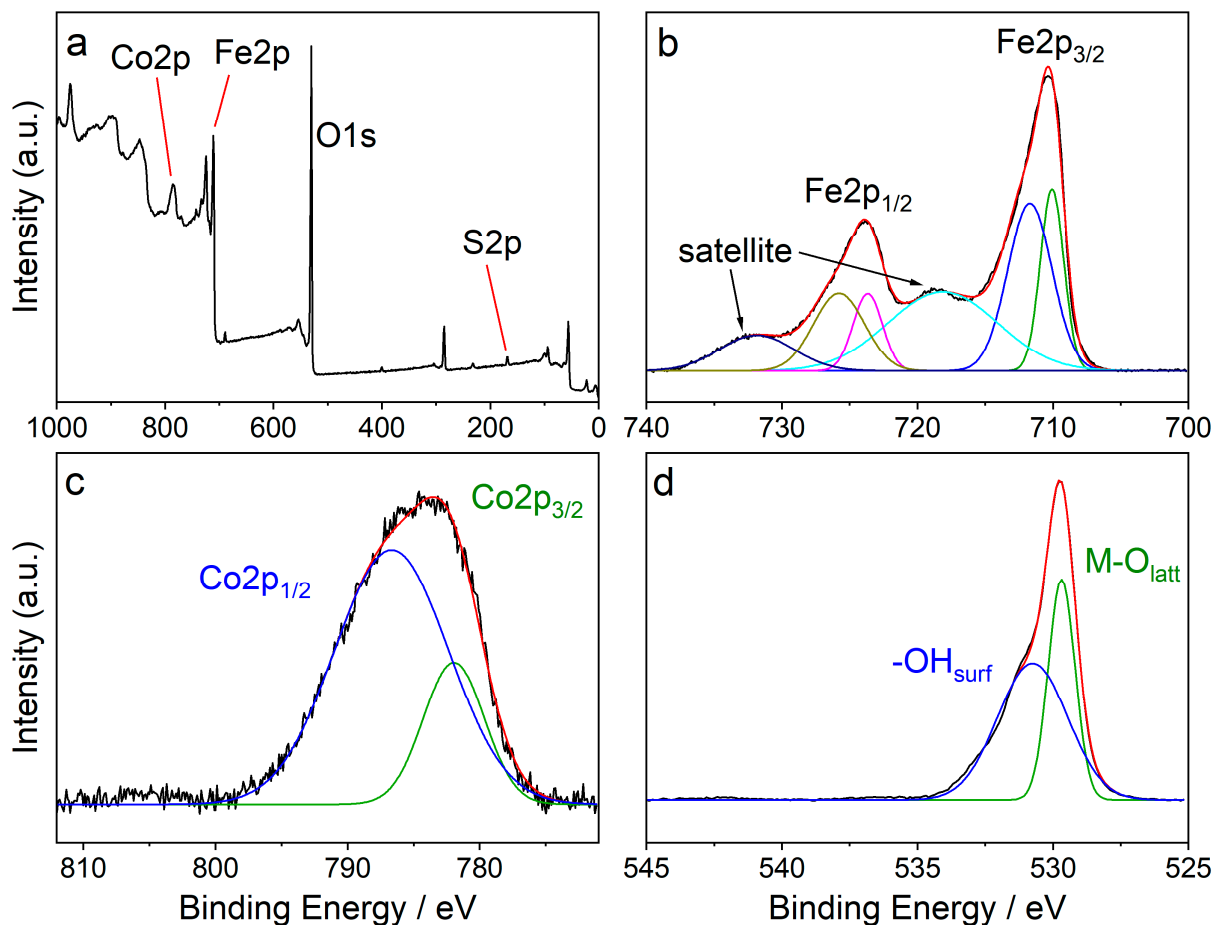


Figure 2. XPS spectra of CFO-AMP in different regions (a) survey, (b) Fe2p, (c) Co2p, and (d) O1s. XPS spectra b–d are background subtracted.

The spectrum of the pristine CFO particles shows exactly the same signals except that the S2p signal is missing, as shown in Figure 3.

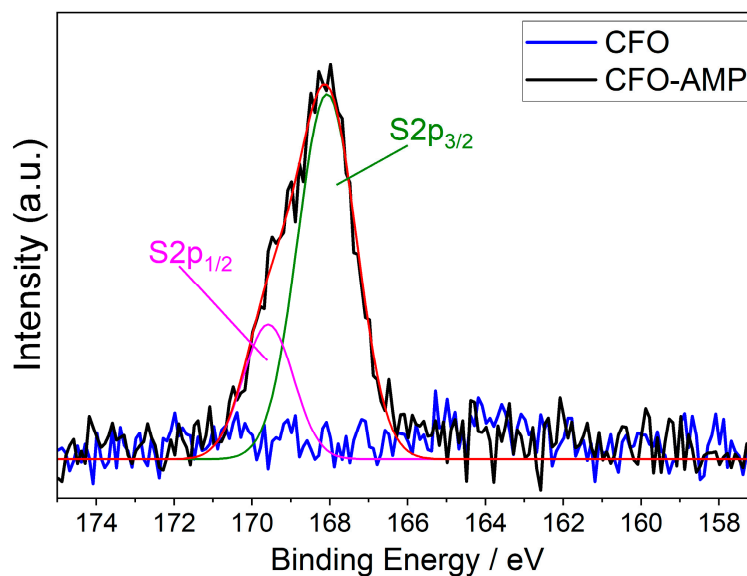


Figure 3. Background-subtracted XPS spectra region of S2p comparing CFO and CFO-AMP.

The S2p high-resolution XPS spectra of CFO-AMP can be deconvoluted into two peaks at 782.0 eV and 786.7 eV, which is an effect of the spin-orbit splitting of S2p_{1/2} and S2p_{3/2}. In the S2p high-resolution XPS spectra of the pristine, unmodified CFO, no signals were observed. The XPS spectra of the pristine CFO and the modified CFO confirm that the surface modification of the CFO nanoparticle was successful. Figure 4a shows the SEM images of CFO nanoparticles. It can be seen that the particles are of uniform, round shape with a narrow size distribution.

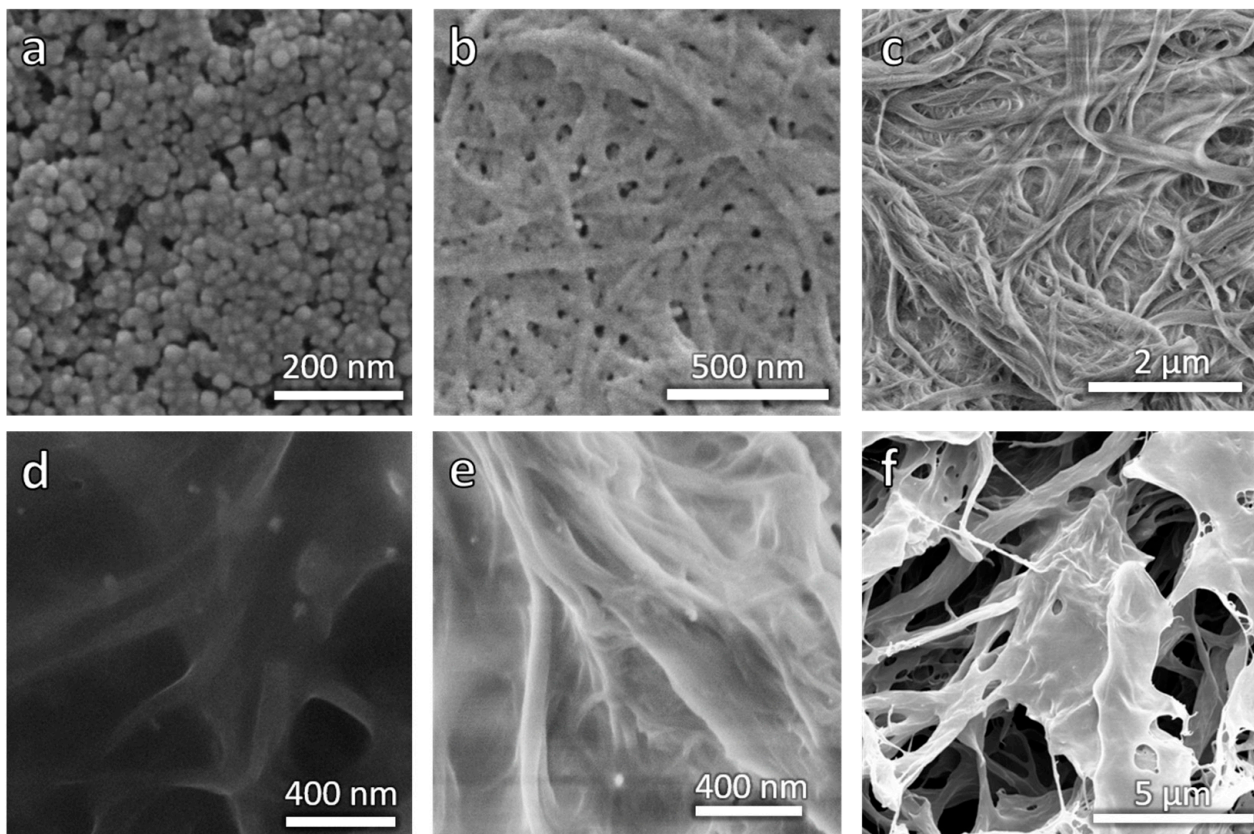


Figure 4. SEM pictures of samples. (a) CFO, (b) CNF-MI, (c) CNF-PSA-CFO, (d) CNF-PSA-CFO, (e) CNF-PSA-CFO, and (f) CNF-PSA-CFO 3D printed, freeze-dried, and cut open. Pictures d and e were taken with the EsB detector.

With the CNF-MI and the CFO-AMP on hand, it was time to let the CNF-based macroinitiator initiate the Cu(0)-mediated SET-LRP of styryl acrylate (SA) in the presence of the modified CFO NPs. The result was a slightly orange/brown but mostly transparent gel in toluene. The color of the gel relies on the presence of the CFO NPs and is a good indication of well-dispersed nanoparticles due to a chemical bond between the particles and the CNF-PSA composite because otherwise, the particles would have been eliminated in the purification process. The morphological appearance has been analyzed with the help of SEM pictures.

When comparing the pictures in Figure 4b,c (CNF-MI and CNF-PSA-CFO), it can be clearly seen that the fibrils of the CNF are still clearly visible when polymer coated, even the cross-linked CFO particles are well observable as bright spots in Figure 4d,e. These pictures were taken with an EsB detector. In this technique, backscattered electrons are measured. The backscattered electrons come from the primary electrons interacting with the nuclei of the sample atoms. These images show a material contrast due to differences in the chemical composition of the sample. Thereby, the intensity of the backscattered signal increases with the atomic number of the atom, resulting in brighter areas in the EsB image corresponding to areas with heavier atoms. Therefore, organic matter appears darker than

inorganic matter, such as metal oxides. Based on the contrast and the present size of the particles, it can be assumed that they are most likely the CFO particles. Therefore, these SEM pictures directly show the polymer modification of the fibrils and the presence of individual nanoparticles as cross-linking agents in the CNF-PSA-CFO gel.

For further analysis, the pristine CNF, the chemical-modified CNF with 2-bromo-2-methylpropionic acid (CNF-MI), and the cross-linked PSA-modified CNF (CNF-PSA-CFO) were monitored with IR (Figure 5).

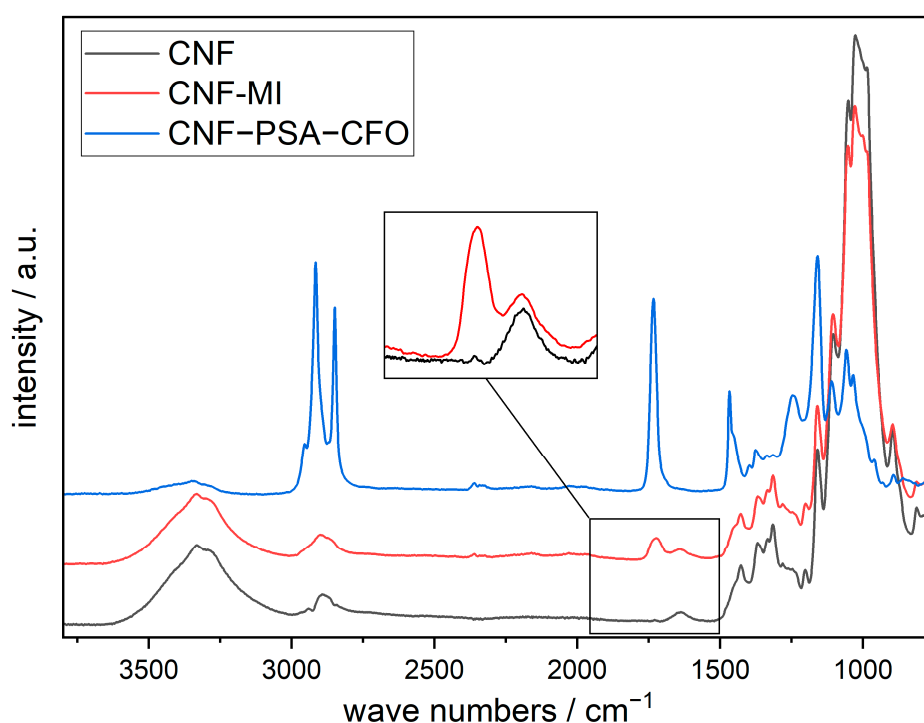


Figure 5. FTIR spectra of pristine CNF, CNF-based macroinitiator (CNF-MI), and poly(SA)-grafted CNF (CNF-PSA-CFO). Data were shifted in intensity by equal amounts for better visualization.

All three spectrums show the CNF characteristic bands localized at 3332 cm^{-1} (O-H), 2900 and 2865 cm^{-1} (C-H), 1428 cm^{-1} (C-H), and 1161 cm^{-1} (C-O-C). In addition, the spectrum of CNF-MI shows an absorption band localized at 1726 cm^{-1} (C=O) attributed to the carbonyl group of the initiator ester function. The spectrum of CNF-PS-CFO shows strong additional absorption bands localized at 2916 and 2849 cm^{-1} (C-H), 1734 cm^{-1} (C=O), 1468 cm^{-1} (C-H), 1161 , and 1246 cm^{-1} (C-O-C) confirming the presence of ester groups and an abundance of methylene groups in the main and side chains of the grafted SA polymer.

To determine the thermal stability and the actual content of CFO nanoparticles in the CNF-PSA-CFO material, TGA measurements were carried out.

The TGA measurement, shown in Figure 6, indicates that CNF-PSA-CFO is thermally stable up to a temperature of around $300\text{ }^{\circ}\text{C}$. Above this temperature, the thermal decomposition takes place and leaves a residue of $1.5\text{ wt}\%$. Since CNF and PSA consist only of organic material, the residual mass is directly the content of CFO nanoparticles.

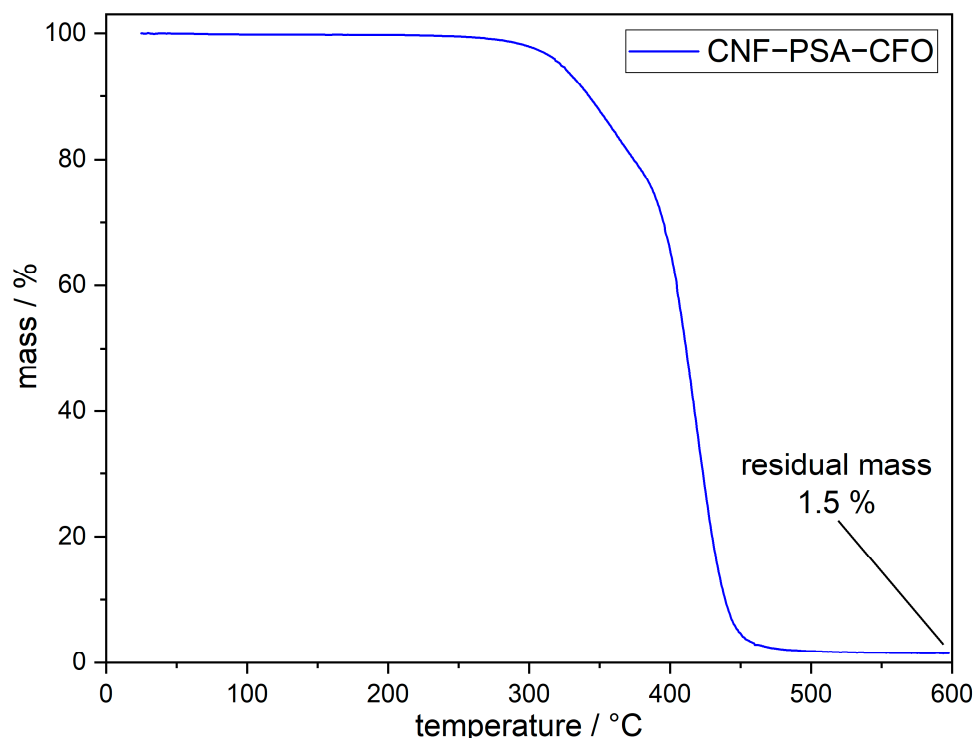


Figure 6. TGA curve of CNF-PSA-CFO under inert nitrogen atmosphere.

Now that we can be sure that the CNF-PSA-CFO material is made of chemically connected CNF and PSA chemically cross-linked with CFO nanoparticles, it is worthwhile to check if the CFO nanoparticles have preserved their functionality and intrinsic properties. CFO nanoparticles are known for their magnetic [67,68] and electrochemical [69] properties. To analyze the magnetic properties of the nanoparticles embedded in CNF-PSA, a vibrating sample magnetometer (VSM) was used.

The VSM measurement in Figure 7 of the CNF-PSA-CFO sample shows the gravimetric magnetization against the external magnetic field strength. The absence of a magnetic hysteresis indicates that the CFO particles in the CNF-PSA-CFO material exhibit superparamagnetic behavior. Mitra et al. found that their CFO nanoparticles have ferromagnetic properties [67]. These particles had a diameter of 50 nm. The particle size of our CFO particles was estimated to be 20–30 nm from SEM images (Figure 4a,b). This small size of our particles is the reason for the superparamagnetic behavior. The gravimetric saturation magnetization with 0.03 emu/g is quite low due to the very low content of CFO in the CNF-PSA-CFO of 1.5 wt%. However, this measurable magnetization of the CNF-PSA-CFO sample shows that the magnetic properties of the CFO still remain and can be used in further applications.

Now that it has been confirmed that the CFO NPs still have their magnetic properties in the CNF-PSA-CFO material, the electrochemical properties can be addressed, and the qualitative electrochemical study on CNF-PSA-CFO provided the following results.

Figure 8 shows the cyclic voltammetry of CNF-PSA-CFO at a platinum electrode in water-free THF. Only one irreversible reduction peak could be observed at $V = -1.14$ V vs. a silver wire as a reference electrode, and the produced current was $I = 0.81$ μ A. No appreciable oxidation peak was observed within the electrochemical window of the solution.

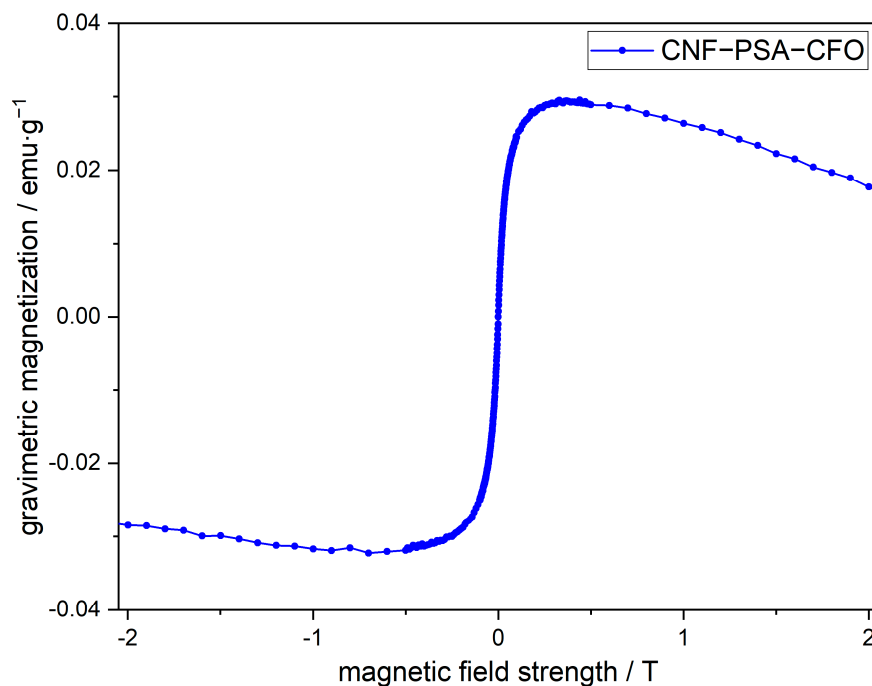


Figure 7. Magnetization as a function of the applied magnetic field of CNF-PSA-CFO.

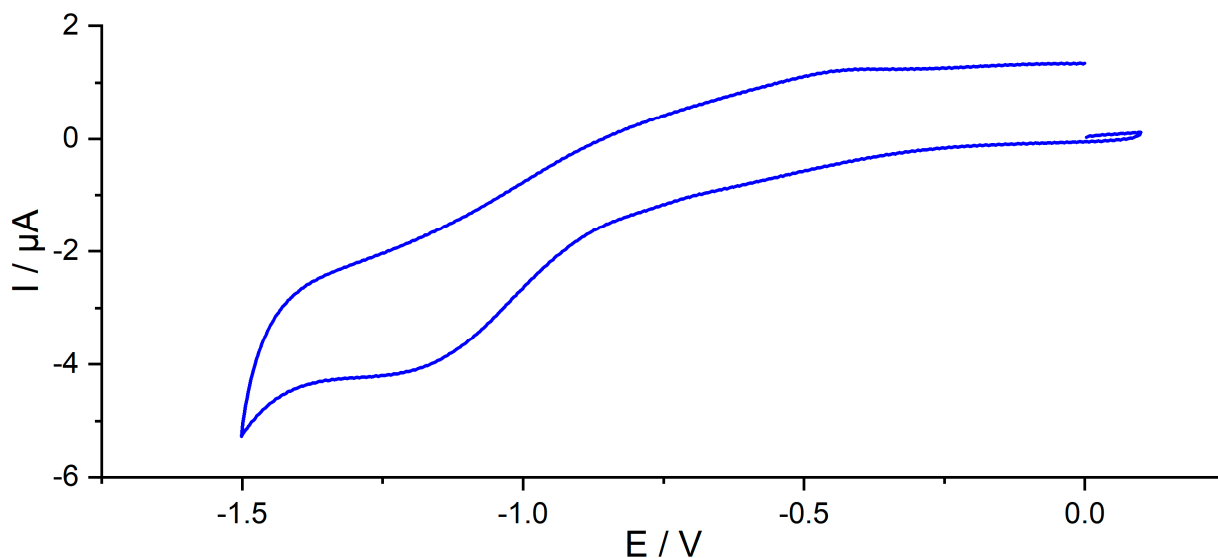


Figure 8. Cyclic voltammogram showing the reduction phase at a platinum electrode of CNF-PSA-CFO ($30 \text{ mg}\cdot\text{L}^{-1}$) in THF ($0.1 \text{ mol}\cdot\text{L}^{-3} \text{ NBu}_4\text{PF}_6$) at 298.15 K . $\nu = 0.1 \text{ V}\cdot\text{s}^{-1}$.

The reduction peak can be explained by the easily reducible nature of the oxidized Fe and Co in the CFO. However, a study conducted by Mylarappa et al. [70] in an aqueous medium shows that CFO undergoes a quasi-reversible reduction and shows a reduction peak at -0.4 V vs. Ag/AgCl reference electrode. In addition, another study conducted by Pereira et al. [71], where they attempted to explore the catalytic effect of CNF-modified electrodes on the reduction of CO_2 , shows that CNFs alone do not undergo any reduction in the electrochemical window of the current study. The low current produced during the CV study is due to the very low solubility of CNF-PSA-CFO in THF. When a full redox scan was performed on the material, a slight oxidation peak was observed at $+0.4 \text{ V}$; the current peak was too low that it could not be taken into consideration. Such an oxidation peak could result from the reoxidation of Fe and Co generated in the medium upon reduction.

With this fully characterized CNF–PSA–CFO sample, we tested its 3D printability. For that, we used an INKREDIBLE 3D printer from the company CELLINK. These printers are able to print any 3D object with gel inks by pneumatic extrusion. We found that a toluene-based gel from the CNF–PSA–CFO material with a solid content of 10 wt% works the best with our material. Some simple shapes were successfully printed with a 0.41 mm stainless steel nozzle and extrusion pressures of 30–50 kPa. We designed a basic $10 \times 10 \times 5$ mm cube and printed this flat on its 10×10 mm surface (Figure 9a,b), as well as on its 5×10 mm surface (Figure 9c,d) to test the gel's performance for 3D printing applications.

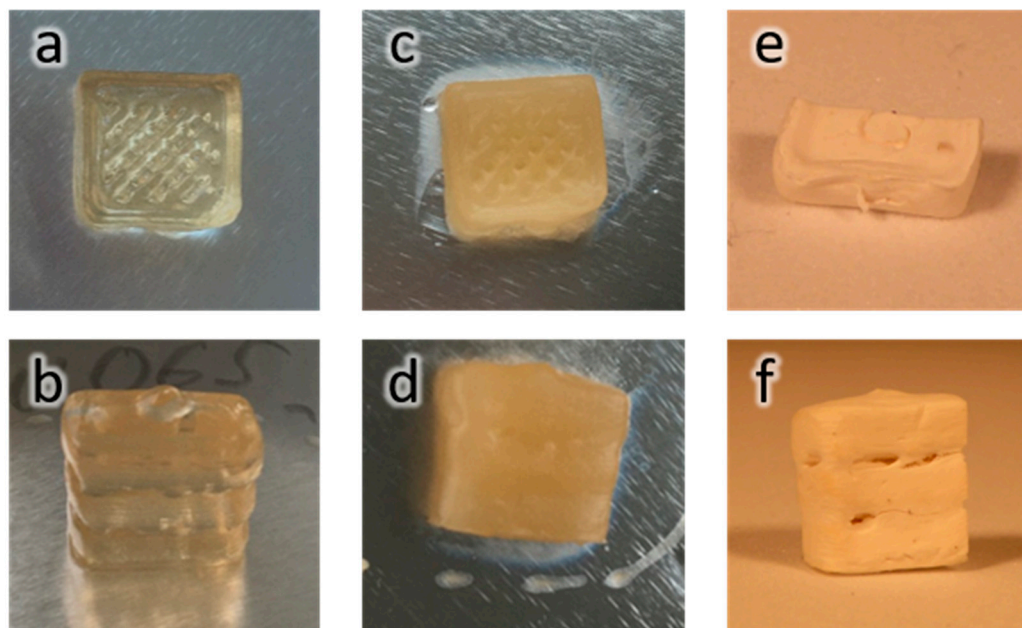


Figure 9. Photos of 3D printed cubes from CNF–PSA–CFO in toluene (10 wt%). The upper row shows the $10 \times 10 \times 5$ mm cube printed on its 10×10 mm surface; the lower row was printed on its 5×10 mm surface. (a,b) Toluene gel after printing, (c,d) DMSO-based gel after the solvent exchange, and (e,f) freeze-dried cubes (cut open for electron microscopy).

The gel performed great in the 3D printing process, and both orientations of the test cube were printed successfully. If the 3D object were dried after printing at high temperature or under ambient conditions, the object would collapse because of the surface tension and capillary forces of toluene in the pores of the gel. To overcome this issue, different drying methods could be applied. One possibility is a solvent exchange followed by supercritical drying with CO_2 , which would lead to a true aerogel [72]. A different but very effective method is freeze-drying. A freeze-dried gel is often named a cryogel. Toluene is not a solvent from which direct freeze-drying is possible, so in the first postprinting step, the toluene has to be solvent-exchanged with DMSO, with which freeze-drying is possible. In Figure 9c,d, the solvent-exchanged cubes are shown. From these pictures, it can be seen that no major shrinkage or deformation due to solvent exchange from toluene to DMSO has occurred. Once the cubes were solvent-exchanged, they were frozen in liquid nitrogen and freeze-dried overnight. Figure 9e,f shows the freeze-dried cryogel cubes. It can be seen that the shape was retained after freeze-drying and, therefore, throughout the entire consolidation and drying process.

4. Conclusions

The conversion of hydrophilic CNF into modified CFO nanoparticle-assisted highly cross-linked hydrophobic network gel with magnetic and electrochemical properties for 3D printing and printed forms was demonstrated in the paper. The successful modifi-

cation of the CFO nanoparticles with 2-Acrylamido-2-methyl-1-propanesulfonic acid by hetero-condensation with CFO surface hydroxyl groups was verified by XPS measurements. Furthermore, the CNF was converted into a CNF-based macroinitiator (CNF-MI) by grafting an initiator unit on the CNF through an esterification reaction with 2-bromo-2-methylpropionic acid. The CNF-MI was then used to initiate a SET-LRP reaction of stearyl acrylate in the presence of modified CFO-AMP, which has led to a hydrophobic CNF-PSA material highly cross-linked with CFO nanoparticles. This material was characterized by SEM, IR, and TGA. To verify the magnetic properties of the CFO particles, a VSM measurement was performed, which confirmed that magnetic functionality was preserved. To ascertain the electrochemical properties of the CNF-PSA-CFO material, cyclic voltammetry measurements were carried out. Only one irreversible reduction peak was observed, which is attributed to the easily reducible nature of the oxidized Fe and Co in the CFO. This is the first hint of the electrochemical behavior of such materials, but further studies should be performed to unravel the capacitance and impedance effect of the material, as well as to determine the electrochemical properties quantitatively. This way, modified electrodes should be prepared using the CNF-PSA-CFO material, and the electrochemical measurements should be performed in an aqueous medium.

In addition, we were able to show that a 10 wt% gel of CNF-PSA-CFO in toluene was great 3D printable with a gel 3D printer using pneumatic extrusion. These 3D printed objects could be solidified through solvent exchange from toluene to DMSO and then freeze-dried under shape retention to give a cryogel.

Author Contributions: Conceptualization, J.B.M. and J.R.G.N.; methodology, J.B.M.; validation, J.B.M. and J.R.G.N.; formal analysis, J.B.M.; investigation, J.B.M.; writing—original draft preparation, J.B.M.; writing—review and editing, J.B.M., S.W., R.K., C.G., B.N. and J.R.G.N.; visualization, J.B.M.; supervision, J.R.G.N.; project administration, J.R.G.N.; funding acquisition, J.R.G.N. All authors have read and agreed to the published version of the manuscript.

Funding: This research was funded by Fachagentur Nachwachsende Rohstoffe e.V. (FNR Project number 2220HV024X).

Data Availability Statement: Not applicable.

Conflicts of Interest: The authors declare no conflict of interest. The funders had no role in the design of the study; in the collection, analyses, or interpretation of data; in the writing of the manuscript; or in the decision to publish the results.

References

1. Thomas, B.; Raj, M.C.; B, A.K.; H, R.M.; Joy, J.; Moores, A.; Drisko, G.L.; Sanchez, C. Nanocellulose, a Versatile Green Platform: From Biosources to Materials and Their Applications. *Chem. Rev.* **2018**, *118*, 11575–11625. [[CrossRef](#)] [[PubMed](#)]
2. Kim, J.-H.; Shim, B.S.; Kim, H.S.; Lee, Y.-J.; Min, S.-K.; Jang, D.; Abas, Z.; Kim, J. Review of Nanocellulose for Sustainable Future Materials. *Int. J. Precis. Eng. Manuf. Technol.* **2015**, *2*, 197–213. [[CrossRef](#)]
3. Shak, K.P.Y.; Pang, Y.L.; Mah, S.K. Nanocellulose: Recent Advances and Its Prospects in Environmental Remediation. *Beilstein J. Nanotechnol.* **2018**, *9*, 2479–2498. [[CrossRef](#)] [[PubMed](#)]
4. Lang, Z.; Ju, Y.; Wang, Y.; Xiao, Z.; Wang, H.; Liang, D.; Li, J.; Xie, Y. Cellulose-Derived Solid-Solid Phase Change Thermal Energy Storage Membrane with Switchable Optical Transparency. *Chem. Eng. J.* **2022**, *435*, 134851. [[CrossRef](#)]
5. Wang, W.; Yu, F.; Ba, Z.; Qian, H.; Zhao, S.; Liu, J.; Jiang, W.; Li, J.; Liang, D. In-Depth Sulfhydryl-Modified Cellulose Fibers for Efficient and Rapid Adsorption of Cr(VI). *Polymers* **2022**, *14*, 1482. [[CrossRef](#)] [[PubMed](#)]
6. Zhao, D.; Pang, B.; Zhu, Y.; Cheng, W.; Cao, K.; Ye, D.; Si, C.; Xu, G.; Chen, C.; Yu, H. A Stiffness-Switchable, Biomimetic Smart Material Enabled by Supramolecular Reconfiguration. *Adv. Mater.* **2022**, *34*, 2107857. [[CrossRef](#)]
7. Zhang, Y.; Nypelö, T.; Salas, C.; Arboleda, J.; Hoeger, I.C.; Rojas, O.J. Cellulose Nanofibrils: From Strong Materials to Bioactive Surfaces. *J. Renew. Mater.* **2013**, *1*, 195–211. [[CrossRef](#)]
8. Voisin, H.; Bergström, L.; Liu, P.; Mathew, A. Nanocellulose-Based Materials for Water Purification. *Nanomaterials* **2017**, *7*, 57. [[CrossRef](#)]
9. Lin, N.; Dufresne, A. Nanocellulose in Biomedicine: Current Status and Future Prospect. *Eur. Polym. J.* **2014**, *59*, 302–325. [[CrossRef](#)]
10. Spence, K.; Habibi, Y.; Dufresne, A. *Cellulose Fibers: Bio- and Nano-Polymer Composites*; Springer: Berlin/Heidelberg, Germany, 2011; ISBN 978-3-642-17369-1.

11. Guo, J.; Filpponen, I.; Su, P.; Laine, J.; Rojas, O.J. Attachment of Gold Nanoparticles on Cellulose Nanofibrils via Click Reactions and Electrostatic Interactions. *Cellulose* **2016**, *23*, 3065–3075. [[CrossRef](#)]
12. Wei, H.; Rodriguez, K.; Renneckar, S.; Leng, W.; Vikesland, P.J. Preparation and Evaluation of Nanocellulose–Gold Nanoparticle Nanocomposites for SERS Applications. *Analyst* **2015**, *140*, 5640–5649. [[CrossRef](#)] [[PubMed](#)]
13. Dadigala, R.; Bandi, R.; Alle, M.; Park, C.-W.; Han, S.-Y.; Kwon, G.-J.; Lee, S.-H. Effective Fabrication of Cellulose Nanofibrils Supported Pd Nanoparticles as a Novel Nanozyme with Peroxidase and Oxidase-like Activities for Efficient Dye Degradation. *J. Hazard. Mater.* **2022**, *436*, 129165. [[CrossRef](#)] [[PubMed](#)]
14. Xue, J.; Song, F.; Yin, X.; Wang, X.; Wang, Y. Let It Shine: A Transparent and Photoluminescent Foldable Nanocellulose/Quantum Dot Paper. *ACS Appl. Mater. Interfaces* **2015**, *7*, 10076–10079. [[CrossRef](#)] [[PubMed](#)]
15. Guo, J.; Liu, D.; Filpponen, I.; Johansson, L.-S.; Malho, J.-M.; Quraishi, S.; Liebner, F.; Santos, H.A.; Rojas, O.J. Photoluminescent Hybrids of Cellulose Nanocrystals and Carbon Quantum Dots as Cytocompatible Probes for in Vitro Bioimaging. *Biomacromolecules* **2017**, *18*, 2045–2055. [[CrossRef](#)] [[PubMed](#)]
16. Khabibullin, A.; Alizadehgiashi, M.; Khuu, N.; Prince, E.; Tebbe, M.; Kumacheva, E. Injectable Shear-Thinning Fluorescent Hydrogel Formed by Cellulose Nanocrystals and Graphene Quantum Dots. *Langmuir* **2017**, *33*, 12344–12350. [[CrossRef](#)]
17. Tang, A.; Liu, Y.; Wang, Q.; Chen, R.; Liu, W.; Fang, Z.; Wang, L. A New Photoelectric Ink Based on Nanocellulose/CdS Quantum Dots for Screen-Printing. *Carbohydr. Polym.* **2016**, *148*, 29–35. [[CrossRef](#)] [[PubMed](#)]
18. Wicklein, B.; Diem, A.M.; Knöller, A.; Cavalcante, M.S.; Bergström, L.; Bill, J.; Burghard, Z. Dual-Fiber Approach toward Flexible Multifunctional Hybrid Materials. *Adv. Funct. Mater.* **2018**, *28*, 1704274. [[CrossRef](#)]
19. Gutierrez, J.; Fernandes, S.C.M.; Mondragon, I.; Tercjak, A. Conductive Photoswitchable Vanadium Oxide Nanopaper Based on Bacterial Cellulose. *ChemSusChem* **2012**, *5*, 2323–2327. [[CrossRef](#)]
20. Olmos-Juste, R.; Guaresti, O.; Calvo-Correas, T.; Gabilondo, N.; Eceiza, A. Design of Drug-Loaded 3D Printing Biomaterial Inks and Tailor-Made Pharmaceutical Forms for Controlled Release. *Int. J. Pharm.* **2021**, *609*, 121124. [[CrossRef](#)]
21. Lim, Y.Y.; Zaidi, A.M.A.; Miskon, A. Composing On-Program Triggers and On-Demand Stimuli into Biosensor Drug Carriers in Drug Delivery Systems for Programmable Arthritis Therapy. *Pharmaceuticals* **2022**, *15*, 1330. [[CrossRef](#)]
22. Navarro, J.R.G.; Edlund, U. Surface-Initiated Controlled Radical Polymerization Approach to Enhance Nanocomposite Integration of Cellulose Nanofibrils. *Biomacromolecules* **2017**, *18*, 1947–1955. [[CrossRef](#)] [[PubMed](#)]
23. Navarro, J.R.G.; Wennmalm, S.; Godfrey, J.; Breitholtz, M.; Edlund, U. Luminescent Nanocellulose Platform: From Controlled Graft Block Copolymerization to Biomarker Sensing. *Biomacromolecules* **2016**, *17*, 1101–1109. [[CrossRef](#)] [[PubMed](#)]
24. Navarro, J.R.G.; Rostami, J.; Ahlinder, A.; Mietner, J.B.; Bernin, D.; Saake, B.; Edlund, U. Surface-Initiated Controlled Radical Polymerization Approach to In Situ Cross-Link Cellulose Nano Fibrils with Inorganic Nanoparticles. *Biomacromolecules* **2020**, *21*, 1952–1961. [[CrossRef](#)] [[PubMed](#)]
25. Dalloul, F.; Mietner, J.B.; Navarro, J.R.G. Production and 3D Printing of a Nanocellulose-Based Nanofibrils and High-Density Polyethylene (HDPE) for the Fabrication of 3D Complex Shapes. *Fibers* **2022**, *10*, 91. [[CrossRef](#)]
26. Percec, V.; Guliashvili, T.; Ladislav, J.S.; Wistrand, A.; Stjern Dahl, A.; Sienkowska, M.J.; Monteiro, M.J.; Sahoo, S. Ultrafast Synthesis of Ultrahigh Molar Mass Polymers by Metal-Catalyzed Living Radical Polymerization of Acrylates, Methacrylates, and Vinyl Chloride Mediated by SET at 25 °C. *J. Am. Chem. Soc.* **2006**, *128*, 14156–14165. [[CrossRef](#)]
27. Rosen, B.M.; Percec, V. Single-Electron Transfer and Single-Electron Transfer Degenerative Chain Transfer Living Radical Polymerization. *Chem. Rev.* **2009**, *109*, 5069–5119. [[CrossRef](#)]
28. Zhang, N.; Samanta, S.R.; Rosen, B.M.; Percec, V. Single Electron Transfer in Radical Ion and Radical-Mediated Organic, Materials and Polymer Synthesis. *Chem. Rev.* **2014**, *114*, 5848–5958. [[CrossRef](#)]
29. Nguyen, N.H.; Levere, M.E.; Kulis, J.; Monteiro, M.J.; Percec, V. Analysis of the Cu(0)-Catalyzed Polymerization of Methyl Acrylate in Disproportionating and Nondisproportionating Solvents. *Macromolecules* **2012**, *45*, 4606–4622. [[CrossRef](#)]
30. Lligadas, G.; Grama, S.; Percec, V. Recent Developments in the Synthesis of Biomacromolecules and Their Conjugates by Single Electron Transfer-Living Radical Polymerization. *Biomacromolecules* **2017**, *18*, 1039–1063. [[CrossRef](#)]
31. Lligadas, G.; Grama, S.; Percec, V. Single-Electron Transfer Living Radical Polymerization Platform to Practice, Develop, and Invent. *Biomacromolecules* **2017**, *18*, 2981–3008. [[CrossRef](#)]
32. Edlund, U.; Albertsson, A.C. SET-LRP Goes “Green”: Various Hemicellulose Initiating Systems under Non-Inert Conditions. *J. Polym. Sci. Part A Polym. Chem.* **2012**, *50*, 2650–2658. [[CrossRef](#)]
33. Edlund, U.; Albertsson, A.-C. Macroinitiator Halide Effects in Galactoglucomannan-Mediated Single Electron Transfer-Living Radical Polymerization. *J. Polym. Sci. Part A Polym. Chem.* **2011**, *49*, 4139–4145. [[CrossRef](#)]
34. Maurya, D.S.; Malik, A.; Feng, X.; Bensabeh, N.; Lligadas, G.; Percec, V. Me₆-TREN/TREN Mixed-Ligand Effect During SET-LRP in the Catalytically Active DMSO Revitalizes TREN into an Excellent Ligand. *Biomacromolecules* **2020**, *21*, 1902–1919. [[CrossRef](#)] [[PubMed](#)]
35. Moreno, A.; Ronda, J.C.; Cádiz, V.; Galià, M.; Lligadas, G.; Percec, V. SET-LRP from Programmed Difunctional Initiators Encoded with Double Single-Cleavage and Double Dual-Cleavage Groups. *Biomacromolecules* **2019**, *20*, 3200–3210. [[CrossRef](#)] [[PubMed](#)]
36. Feng, X.; Maurya, D.S.; Bensabeh, N.; Moreno, A.; Oh, T.; Luo, Y.; Lejnicks, J.N.; Galià, M.; Miura, Y.; Monteiro, M.J.; et al. Replacing Cu(II)Br₂ with Me₆-TREN in Biphasic Cu(0)/TREN Catalyzed SET-LRP Reveals the Mixed-Ligand Effect. *Biomacromolecules* **2020**, *21*, 250–261. [[CrossRef](#)]

37. Zhang, Q.; Wilson, P.; Li, Z.; McHale, R.; Godfrey, J.; Anastasaki, A.; Waldron, C.; Haddleton, D.M. Aqueous Copper-Mediated Living Polymerization: Exploiting Rapid Disproportionation of CuBr with Me6TREN. *J. Am. Chem. Soc.* **2013**, *135*, 7355–7363. [[CrossRef](#)]
38. Anastasaki, A.; Nikolaou, V.; Nurumbetov, G.; Wilson, P.; Kempe, K.; Quinn, J.F.; Davis, T.P.; Whittaker, M.R.; Haddleton, D.M. Cu(0)-Mediated Living Radical Polymerization: A Versatile Tool for Materials Synthesis. *Chem. Rev.* **2015**, *116*, 835–877. [[CrossRef](#)]
39. Samanta, S.R.; Nikolaou, V.; Keller, S.; Monteiro, M.J.; Wilson, D.A.; Haddleton, D.M.; Percec, V. Aqueous SET-LRP Catalyzed with “in Situ” Generated Cu(0) Demonstrates Surface Mediated Activation and Bimolecular Termination. *Polym. Chem.* **2015**, *6*, 2084–2097. [[CrossRef](#)]
40. Waldron, C.; Zhang, Q.; Li, Z.; Nikolaou, V.; Nurumbetov, G.; Godfrey, J.; McHale, R.; Yilmaz, G.; Randev, R.K.; Girault, M.; et al. Absolut “Copper Catalyzation Perfected”; Robust Living Polymerization of NIPAM: Guinness Is Good for SET-LRP. *Polym. Chem.* **2014**, *5*, 57–61. [[CrossRef](#)]
41. Rees, A.; Powell, L.C.; Chinga-Carrasco, G.; Gethin, D.T.; Syverud, K.; Hill, K.E.; Thomas, D.W. 3D Bioprinting of Carboxymethylated-Periodate Oxidized Nanocellulose Constructs for Wound Dressing Applications. *Biomed Res. Int.* **2015**, *2015*, 925757. [[CrossRef](#)]
42. Kolan, K.; Liu, Y.; Baldrige, J.; Murphy, C.; Semon, J.; Day, D. Solvent Based 3D Printing of Biopolymer / Bioactive Glass Composite and Hydrogel for Tissue Engineering Applications. *Procedia CIRP* **2017**, *65*, 38–43. [[CrossRef](#)]
43. Fina, F.; Goyanes, A.; Madla, C.M.; Awad, A.; Sarah, J.; Kuek, J.M.; Patel, P.; Gaisford, S.; Basit, A.W. 3D Printing of Drug-Loaded Gyroid Lattices Using Selective Laser Sintering. *Int. J. Pharm.* **2018**, *547*, 44–52. [[CrossRef](#)] [[PubMed](#)]
44. Arafat, B.; Wojsz, M.; Isreb, A.; Forbes, R.T.; Isreb, M.; Ahmede, W.; Arafat, T.; Alhnan, M.A. Tablet Fragmentation without a Disintegrant: A Novel Design Approach for Accelerating Disintegration and Drug Release from 3D Printed Cellulosic Tablets. *Eur. J. Pharm. Sci.* **2018**, *118*, 191–199. [[CrossRef](#)] [[PubMed](#)]
45. Håkansson, K.M.O.; Henriksson, I.C.; De, C.; Vázquez, P.; Kuzmenko, V.; Markstedt, K.; Enoksson, P.; Gatenholm, P. Solidification of 3D Printed Nanofibril Hydrogels into Functional 3D Cellulose Structures. *Adv. Mater. Technol.* **2016**, *1*, 1600096. [[CrossRef](#)]
46. Markstedt, K.; Escalante, A.; Toriz, G.; Gatenholm, P. Biomimetic Inks Based on Cellulose Nanofibrils and Cross-Linkable Xylans for 3D Printing. *ACS Appl. Mater. Interfaces* **2017**, *9*, 40878–40886. [[CrossRef](#)] [[PubMed](#)]
47. Sultan, S.; Siqueira, G.; Zimmermann, T.; Mathew, A.P. 3D Printing of Nano-Cellulosic Biomaterials for Medical Applications. *Curr. Opin. Biomed. Eng.* **2017**, *2*, 29–34. [[CrossRef](#)]
48. Françon, H.; Wang, Z.; Marais, A.; Mystek, K.; Piper, A.; Granberg, H.; Malti, A.; Gatenholm, P.; Larsson, P.A.; Wågberg, L. Ambient-Dried, 3D-Printable and Electrically Conducting Cellulose Nanofiber Aerogels by Inclusion of Functional Polymers. *Adv. Funct. Mater.* **2020**, *30*, 1909383. [[CrossRef](#)]
49. Mohan, D.; Khairullah, N.F.; How, Y.P.; Sajab, M.S.; Kaco, H. 3D Printed Laminated CaCO₃-Nanocellulose Films as Controlled-Release 5-Fluorouracil. *Polymers* **2020**, *12*, 986. [[CrossRef](#)]
50. Auvinen, V.-V.; Virtanen, J.; Merivaara, A.; Virtanen, V.; Laurén, P.; Tuukkanen, S.; Laaksonen, T. Modulating Sustained Drug Release from Nanocellulose Hydrogel by Adjusting the Inner Geometry of Implantable Capsules. *J. Drug Deliv. Sci. Technol.* **2020**, *57*, 101625. [[CrossRef](#)]
51. Markstedt, K.; Mantas, A.; Tournier, I.; Ha, D.; Gatenholm, P. 3D Bioprinting Human Chondrocytes with Nanocellulose— Alginate Bioink for Cartilage Tissue Engineering Applications. *Biomacromolecules* **2015**, *16*, 1489–1496. [[CrossRef](#)]
52. Leppiniemi, J.; Lahtinen, P.; Paajanen, A.; Mahlberg, R.; Metsä-Kortelainen, S.; Pinomaa, T.; Pajari, H.; Vikholm-Lundin, I.; Pursula, P.; Hytönen, V.P. 3D-Printable Bioactivated Nanocellulose-Alginate Hydrogels. *ACS Appl. Mater. Interfaces* **2017**, *9*, 21959–21970. [[CrossRef](#)] [[PubMed](#)]
53. Li, Y.; Zhu, H.; Wang, Y.; Ray, U.; Zhu, S.; Dai, J.; Chen, C.; Fu, K.; Jang, S.-H.; Henderson, D.; et al. Cellulose-Nanofiber-Enabled 3D Printing of a Carbon-Nanotube Microfiber Network. *Small Methods* **2017**, *1*, 1700222. [[CrossRef](#)]
54. Mietner, J.B.; Jiang, X.; Edlund, U.; Saake, B.; Navarro, J.R.G. 3D Printing of a Bio-Based Ink Made of Cross-Linked Cellulose Nanofibrils with Various Metal Cations. *Sci. Rep.* **2021**, *11*, 6461. [[CrossRef](#)]
55. Chen, W.; Yu, H.; Lee, S.Y.; Wei, T.; Li, J.; Fan, Z. Nanocellulose: A Promising Nanomaterial for Advanced Electrochemical Energy Storage. *Chem. Soc. Rev.* **2018**, *47*, 2837–2872. [[CrossRef](#)] [[PubMed](#)]
56. Shanmugavani, A.; Kalpana, D.; Selvan, R.K. Electrochemical Properties of CoFe₂O₄ Nanoparticles as Negative and Co(OH)₂ and Co₂Fe(CN)₆ as Positive Electrodes for Supercapacitors. *Mater. Res. Bull.* **2015**, *71*, 133–141. [[CrossRef](#)]
57. Sankar, K.V.; Selvan, R.K.; Meyrick, D. Electrochemical Performances of CoFe₂O₄ Nanoparticles and a RGO Based Asymmetric Supercapacitor. *RSC Adv.* **2015**, *5*, 99959–99967. [[CrossRef](#)]
58. Liu, Q.; Kang, X.; Xing, L.; Ye, Z.; Yang, Y. A Facile Synthesis of Nanostructured CoFe₂O₄ for the Electrochemical Sensing of Bisphenol A. *RSC Adv.* **2020**, *10*, 6156–6162. [[CrossRef](#)]
59. He, Q.; Rui, K.; Chen, C.; Yang, J.; Wen, Z. Interconnected CoFe₂O₄-Polypyrrole Nanotubes as Anode Materials for High Performance Sodium Ion Batteries. *ACS Appl. Mater. Interfaces* **2017**, *9*, 36927–36935. [[CrossRef](#)]
60. Karthigayan, N.; Manimuthu, P.; Priya, M.; Sagadevan, S. Synthesis and Characterization of NiFe₂O₄, CoFe₂O₄ and CuFe₂O₄ Thin Films for Anode Material in Li-Ion Batteries. *Nanomater. Nanotechnol.* **2017**, *7*, 1847980417711084. [[CrossRef](#)]
61. Zhang, Q.; Chan, K.-Y.; Quirke, N. Molecular Dynamics Simulation of Water Confined in a Nanopore of Amorphous Silica. *Mol. Simulat.* **2009**, *35*, 1215–1223. [[CrossRef](#)]

62. Macedo, V.M.; Pereira, N.; Tubio, C.R.; Martins, P.; Costa, C.M.; Lanceros-Mendez, S. Carrageenan Based Printable Magnetic Nanocomposites for Actuator Applications. *Compos. Sci. Technol.* **2022**, *224*, 109485. [[CrossRef](#)]
63. Salunkhe, A.B.; Khot, V.M.; Ruso, J.M.; Patil, S.I. Water Dispersible Superparamagnetic Cobalt Iron Oxide Nanoparticles for Magnetic Fluid Hyperthermia. *J. Magn. Magn. Mater.* **2016**, *419*, 533–542. [[CrossRef](#)]
64. Kim, P.; Jones, S.C.; Hotchkiss, P.J.; Haddock, J.N.; Kippelen, B.; Marder, S.R.; Perry, J.W. Phosphonic Acid-Modified Barium Titanate Polymer Nanocomposites with High Permittivity and Dielectric Strength. *Adv. Mater.* **2007**, *19*, 1001–1005. [[CrossRef](#)]
65. Zhu, K.; Jin, C.; Klencsár, Z.; Ganeshraja, A.S.; Wang, J. Cobalt-Iron Oxide, Alloy and Nitride: Synthesis, Characterization and Application in Catalytic Peroxymonosulfate Activation for Orange II Degradation. *Catalysts* **2017**, *7*, 138. [[CrossRef](#)]
66. Rajan, A.; Sharma, M.; Sahu, N.K. Assessing Magnetic and Inductive Thermal Properties of Various Surfactants Functionalised Fe₃O₄ Nanoparticles for Hyperthermia. *Sci. Rep.* **2020**, *10*, 15045. [[CrossRef](#)] [[PubMed](#)]
67. Zhang, J.X.; Dai, J.Y.; So, L.C.; Sun, C.L.; Lo, C.Y.; Or, S.W.; Chan, H.L.W. The Effect of Magnetic Nanoparticles on the Morphology, Ferroelectric, and Magnetolectric Behaviors of CFO/P(VDF-TrFE) 0-3 Nanocomposites. *J. Appl. Phys.* **2009**, *105*, 054102. [[CrossRef](#)]
68. Olsson, R.T.; Azizi Samir, M.A.S.; Salazar-Alvarez, G.; Belova, L.; Ström, V.; Berglund, L.A.; Ikkala, O.; Nogués, J.; Gedde, U.W. Making Flexible Magnetic Aerogels and Stiff Magnetic Nanopaper Using Cellulose Nanofibrils as Templates. *Nat. Nanotechnol.* **2010**, *5*, 584–588. [[CrossRef](#)]
69. Mitra, S.; Veluri, P.S.; Chakraborty, A.; Petla, R.K. Electrochemical Properties of Spinel Cobalt Ferrite Nanoparticles with Sodium Alginate as Interactive Binder. *ChemElectroChem* **2014**, *1*, 1068–1074. [[CrossRef](#)]
70. Mylarappa, M.; Venkata Lakshmi, V.; Vishnu Mahesh, K.R.; Raghavendra, N.; Nagaswarupa, H.P. Cyclic Voltammetry, Impedance and Thermal Properties of CoFe₂O₄ Obtained from Waste Li-Ion Batteries. *Mater. Today Proc.* **2018**, *5*, 22425–22432. [[CrossRef](#)]
71. Pereira, R.V.; Gallina, T.E.; Pereira-da-Silva, M.A.; Freitas, K.S.; de Menezes, A.J. Electrochemical Behavior of Cellulose Nanofibrils Functionalized with Dicyanovinyl Groups. In *Nanofibers-Synthesis, Properties and Applications*; IntechOpen: London, UK, 2021; Volume 32, pp. 137–144.
72. Heath, L.; Thielemans, W. Cellulose Nanowhisker Aerogels. *Green Chem.* **2010**, *12*, 1448–1453. [[CrossRef](#)]

Disclaimer/Publisher's Note: The statements, opinions and data contained in all publications are solely those of the individual author(s) and contributor(s) and not of MDPI and/or the editor(s). MDPI and/or the editor(s) disclaim responsibility for any injury to people or property resulting from any ideas, methods, instructions or products referred to in the content.